Dynamic behavior of ultra large graphene-based membranes using electrothermal transduction

Dynamic behavior of ultra large graphene-based membranes using electrothermal transduction

A. Al-mashaal[1,a)] G. S. Wood[1)] A. Torin[2)] E. Mastropaolo[1)] M. J. Newton[2)] and R. Cheung[1)]

[1]*School of Engineering, Institute for Integrated Micro and Nano Systems, University of Edinburgh, Edinburgh EH9 3FF, UK*

[2]*Acoustics and Audio Group, University of Edinburgh, Edinburgh EH9 3JZ, UK*

This letter reports an experimental study of an electrothermal actuator made from ultra-large graphene-based bilayer thin film with a diameter to thickness aspect ratio of ~ 10,000. Suspended thin films consisting of multilayer graphene and 350 – 500 nm-thick Poly(methyl methacrylate) (PMMA) have been transferred over circular cavities with a diameter of 3.5 mm. The use of bilayer materials with different mechanical and thermal properties results in thin film structures that can be induced to vibrate mechanically under electrothermal transduction mechanism. The dynamic response of the bilayer has been investigated electrothermally by driving the structures with a combination of alternating current (AC) and direct current (DC) actuation voltages (V_{ac} and V_{dc}) and characterizing their resonant frequencies. It has been found that the bilayer thin film structure behaves as a membrane. In addition, the actuation configurations affect not only the amplitude of vibration, but also the tuning of the resonant frequency of the vibrating membranes. The existence of Joule heating-induced tension lowers the mechanical stiffness of the membrane and hence shifts the resonant frequency downwards by –108187 ppm. A resonant frequency of 3.26 kHz with a vibration amplitude of 4.34 nm has been achieved for 350 nm-thick membranes under actuation voltages of 1 V of V_{ac} and 8 V of V_{dc}.

Graphene-based structures are used widely in many micro- and nanoelectromechanical systems (MEMS/NEMS) technologies. The fascinating properties of graphene have attracted the attention of the scientific community and industrial sector and opened doors for a wide range of potential applications such as electromechanical resonators[1], electromechanical actuators[2], pressure sensors[3], biosensors[4], microphones[5], loudspeakers[6] and microdrums[7]. Mechanically, graphene has remarkable Young's modulus (~ 0.5 – 1 TPa), high mechanical strength (~ 130 GPa), and ultra-low mass density (2200 kg/m^3) that make it an ideal material for the realization of large suspended structures. From an operation point of view, graphene-based devices have been driven/actuated mainly either

[a] Author to whom correspondence should be addressed. Electronic mail: asaad.al@ed.ac.uk , asaad.edaan@uobasrah.edu.iq.

electrostatically[6,8] or acoustically[5,9]. Despite their advantages, these actuation techniques have limitations. For example, nonlinearity, short circuiting, and large driving voltage are the main limitations of the electrostatically driven mechanism[10]. In acoustic actuation, sound pressure and acoustical field sensitivities influence the frequency response of the device significantly[11]. Electrothermal actuation, on the other hand, has the advantages of possessing simple design, achieving relatively large driving displacement when operated under low actuation voltage and therefore can be very efficient for vibration excitation. Compared to other materials, graphene has superior thermal conductivity ($\sim 2000 - 5300$ W/mK)[12,13] and negative coefficient of thermal expansion (CTE $\sim -7 \times 10^{-6}$ K^{-1})[2,12] that make it a promising material for electrothermal actuation. When graphene is integrated with another material with different CTE, the graphene layer may act as a heating and conduction thin film simultaneously. In this case, when the whole bilayer structure is heated, the different CTE of the layers in the bilayer structure will cause an out-of-plane mechanical displacement. Therefore, the bilayer structure will vibrate at its resonant frequencies and achieve maximum displacement at a given actuation input. A few studies have been reported on graphene-based thermal actuator nanostructures such as cantilevers[2], films[14] and plates[15].

In this work, we report the realization of a resonator based on electrothermally-driven and mechanically vibrating graphene/PMMA bilayer structures. Ultra-large suspended thin films of multilayer graphene supported by a thin layer of PMMA have been transferred over a cavity with a diameter of 3.5 mm. The transfer process results in high yield without degrading the mechanical properties or rupturing the surface of the suspended structures. Importantly, the use of only graphene, with a thickness of a few layers and high Young's modulus, will vibrate at high frequency and might not be suitable for some applications. Therefore, employing the PMMA film that has lower density and elasticity than graphene as a second layer could enhance the durability of the membranes and lower the frequency band. In addition, in order to examine the optimal driving configuration that could produce higher vibration amplitude and better sensitivity, the design of our device includes different configurations of actuation electrodes underneath the bilayer structure. In general, this work reveals the bilayer device behaving as a membrane structure, and reports the study of the influence of electrothermal biasing configurations, tension and membrane thickness, on the resonant frequency and the amplitude of vibration of the bilayer structure.

Figure 1 shows the final structure of the electrothermal actuator. To prepare the desired substrate, 250 nm of plasma-enhanced chemical vapour deposition (PECVD) silicon dioxide (SiO_2) has been deposited on a p-type silicon substrate. Then, a layer of 500 nm of aluminum has been patterned by the lift-off process to create multi actuation electrodes. The purpose of using multi actuation electrodes with different configuration to drive the bilayer films is to examine the influence of electrode configuration on the resonant frequency and the amplitude of vibration. Afterwards, a photoresist has been spin coated and patterned photolithographically to define cavities in circular shape. Subsequently, deep reactive ion etching (DRIE) technique has been used to etch the oxide and throughout the whole depth of the substrate. The resultant substrate has circular cavity of 380 µm in depth and 3.5 mm in diameter. Multilayer graphene and thin film of PMMA have been used to prepare the bilayer membranes. First, to transfer ~ 8 layers (~ 2.5 nm) of chemically vapor deposited (CVD) graphene from its copper metal substrate to the desired substrate, PMMA film with thicknesses of 350, 400, and 500 nm has been spin coated on the graphene/copper to act as a supporting layer during and after the transfer. The thickness of 8 layers graphene has been determined by Raman spectroscopy while the thickness of PMMA has been measured with spectroscopic reflectometry. After etching the copper with ferric chloride ($FeCl_3$), the graphene/PMMA thin film has been transferred to the pre-patterned SiO_2/Si substrate. Figure 1.b shows an optical image of the actuator after transferring graphene/PMMA thin film over the cavity.

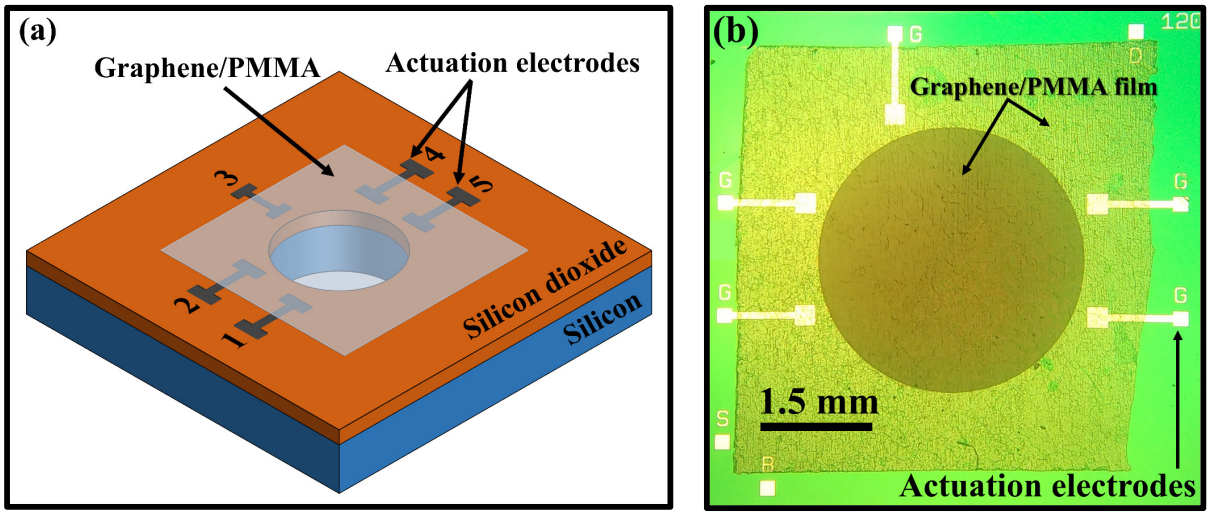

FIG. 1. Schematic illustration (a) and optical image (b) of the electrothermal actuator made from graphene/PMMA thin films.

The graphene/PMMA thin films have been actuated electrothermally by applying a combination of V_{ac} and V_{dc} voltages to the actuation metal electrodes underneath the thin film. In electrothermal actuation, a physical expansion

is induced by a local increase of temperature from Joule heating phenomenon. When the actuation voltage is applied between any two electrodes (as shown in Fig. 1), the current flowing through the bilayer structure will generate heat. Due to the difference in the materials' CTE, a temperature gradient ΔT is induced which produces a thermal stress in the bilayer structure. The induced thermal stress alters the mechanical stiffness of the bilayer structure and forces the entire structure to expand or contract accordingly. In this way of actuation, the graphene/PMMA thin films can be driven into resonance and their frequencies can be tuned (see supplementary material). The resonant frequencies of the bilayer thin films have been measured using a laser Doppler vibrometer (LDV). The measurements have been performed at atmospheric pressure and room temperature conditions. For all measurements, a sweeping excitation signal (100 Hz - 30 kHz) has been applied and a discrete Fourier transform (FFT) has been used to locate the first three modal frequencies of the suspended films. To measure the amplitude of the vibration, a sinusoidal signal has been applied at the resonant frequency modes.

Figure 2 shows the first three measured modes of resonance for the circular thin films as a function of film thickness using electrothermal actuation voltages of 1 V of V_{ac} and 8 V of V_{dc}. For thin films with thickness of 350 nm, for example, the first three resonant frequencies corresponding to (0, 1), (1, 1) and (0, 2) modes have been found to be 3.26, 12.56, and 21.70 kHz respectively (see supplementary material). In the case of thick films with thickness of 500 nm, the first three resonant frequencies have been measured to be 4.64, 16.75, and 26.68 kHz respectively. From the measurements, it can be seen that the resonant frequency of the thin films increases linearly with the film thickness. However, our measurements of the resonant frequencies are much higher than the existing plate model[9] that describes bilayer films (see supplementary material). On the other hand, the existing membrane model that describes the resonant frequency of monolayer[16] or multilayer circular thin film[5,17–19] could be used to model our bilayer system:

$$f_{mn}\,(membrane) = \frac{\alpha_{mn}}{2\pi R}\sqrt{\frac{N}{\rho t}} \tag{1}$$

where R is the radius of the membrane, t is the total thickness of the membrane, ρ is the density of the material, N is the initial pre-tension in the membrane, and α_{mn} is dimensionless coefficient of the resonant mode (m, n are the number of nodal lines).

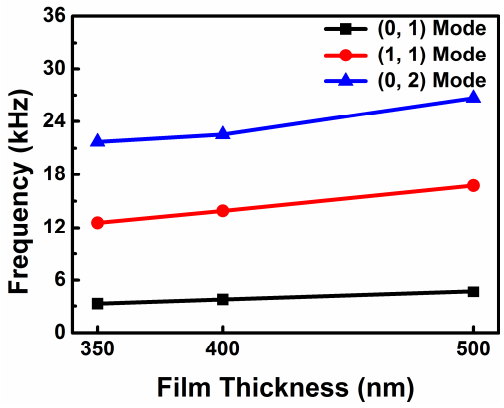

FIG. 2. Measurements of the first three modal resonant frequencies of circular thin films with respect to the film thickness; lines act as guide.

In our bilayer system, equation (1) has been modified to describe the bilayer membrane that is composed of two different materials, by using the effective values of thickness (t_{eff}) and density (ρ_{eff}) for graphene (g) and PMMA (p) as follows:

$$t_{eff} = t_g + t_p \tag{2}$$

$$\rho_{eff} = \frac{\rho_g t_g + \rho_p t_p}{t_g + t_p} \tag{3}$$

In addition to the initial pre-tension (N_i), in our actuation configuration, the Joule heating will induce thermal tension (N_t) to the membrane during electrothermal actuation. Therefore, the resonant frequency of the clamped bilayer circular membrane can be re-written as follows:

$$f_{mn}(membrane) = \frac{\alpha_{mn}}{2\pi R}\sqrt{\frac{N_i + N_t}{\rho_{eff}\, t_{eff}(1 + A_m)}} \tag{4}$$

Since the measurements have been performed in an air medium with a density ρ_{air}, a term describing the additional air mass ($A_m = 2\rho_{air}R/3\,\rho_{eff}t_{eff}$)[20] has been included in our model.

If we assume that the bilayer structures, despite their thicknesses, have the same magnitude of tension, their resonant frequencies should decrease with the increase of the thickness. However, the measurements in Fig. 2 have shown that the resonant frequency increases with the increase of the film thickness. It is possible that such behavior could be attributed to the differences of tension in the membranes. As the membrane tension increases, the resonant

frequency increases. Therefore, different values of total tension ($N_i + N_t$) have been applied in the membrane model (equation 4) to find the values of tension at which the experimental resonant frequency fits with the analytical model. The calculations are presented in Table I. It can be seen that the estimated tension increases with the membrane thickness. This tension represents both the pre-tension and thermal induced tension. In practice, the pre-tension arises from the fabrication and transfer processes, while the thermal induced tension is more likely to be produced from the electrothermal actuation. The magnitude of the total estimated tension in this work is relatively small compared to the tension reported for multilayer graphene membrane[5]. It is worth pointing out that when the thermal induced stress is included in the plate model, the measurements agree with the model only when extremely high magnitude of thermal stresses (135.53 GPa for 350 nm-thick film to 298.43 GPa for 500 nm-thick film) are used (see supplementary material). Therefore, it is concluded that the bilayer film in this work is behaving as a membrane structure rather than a conventional plate.

Table I. Estimation of the magnitude of total tension ($N_i + N_t$) and strain in the graphene/PMMA films with different thicknesses based on the experimental measurements and analytical description in equation (4) for the first resonant frequency ($f_{0,1}$). The strain has been calculated based on the estimated values of tension. The physical properties of Young's modulus and density used in the calculations are respectively 1 TPa and 2270 kg/m^3 for graphene and 3.8 GPa and 1045 kg/m^3 for PMMA.

Graphene/ PMMA Thickness	**Analytical**			**Experimental**
	Tension (N/m)	**Strain**	$f_{0,1}$ (kHz)	$f_{0,1}$ (kHz)
8 layers/ 350 nm	0.801	1.96×10^{-4}	3.26	3.26
8 layers/ 400 nm	1.078	2.52×10^{-4}	3.73	3.73
8 layers/ 500 nm	2.079	4.46×10^{-4}	4.64	4.64

In electrothermal actuation, the driving configurations may have an impact on the resonant frequency and the amplitude of vibration. Figure 3 shows the dynamic response of 350 nm-thick circular membranes to different biasing configurations under constant actuation voltages ($V_{ac} = 1$ V, $V_{dc} = 8$ V). In this case, the actuation voltages have been applied between two fixed metal electrodes using the following configurations (V_{2-4}, V_{2-5}, V_{3-5}, V_{3-4}, V_{4-5}), as shown in Fig. 1(a). It can be observed that the configuration of the actuation has a significant impact on the vibration amplitude and frequency shift of the membranes. The configuration V_{2-4} has shown the largest amplitude of vibration for the first, second and third resonant frequencies compared to the other configurations. The shapes of the measured modes are shown in the supplementary material. At the first resonant frequency, for example, the amplitude of vibration using the shorter path configuration V_{4-5} has been found to be ~ 0.65 nm, which is six times less than the highest amplitude of 4.34 nm using the configuration V_{2-4}. In addition, the electrothermal actuation measurements

have shown a shift in the resonant frequencies as the driving configuration changes, as depicted in Fig. 3(b). For the same configurations, a gradual increase in the vibration amplitude is accompanied by a gradual decrease of the fundamental resonant frequency from 3.42 kHz to 3.05 kHz (−108187 ppm). This observation is suggestive of the fact that depending on the degree of heat generated, a certain electrode configuration can cause both a progressively higher amplitude and a higher frequency shift to lower frequencies, consistent with the existence of thermally induced tension in the membrane.

At the second resonant mode, however, it can be seen from Fig. 3a that the configurations V_{2-4} and V_{3-4} have produced larger amplitudes of vibration than the configurations V_{2-5}, V_{3-5} and V_{4-5}. The second mode (1, 1) has movable parts (anti-nodal points) and immovable parts (nodal points). The immovable nodal points are one diametric node and one concentric node (see the supplementary material). In the V_{2-4} and V_{3-4} configurations, it is likely that the electrical current is flowing in the path of the anti-nodal points, and is being able to heat around the anti-nodal area more, thus inducing a larger amplitude of vibration. In the V_{2-5}, V_{3-5} and V_{4-5} configurations, on the other hand, it is believed that the current is flowing in the path of either the diametric node or the concentric node, and hence will result in a small amplitude of vibration.

From these observations, it is concluded that the best actuation configuration is the one at which the current flows through the largest area of the membrane. Therefore, the design of the actuation electrodes can be further optimized. For example, two large electrodes with arch-like shape could be considered an optimum design that might provide an efficient actuation configuration for circular membranes. In general, the resonant frequency and the amplitude of vibration of the membranes can be tuned by driving the membranes with a certain biasing configuration.

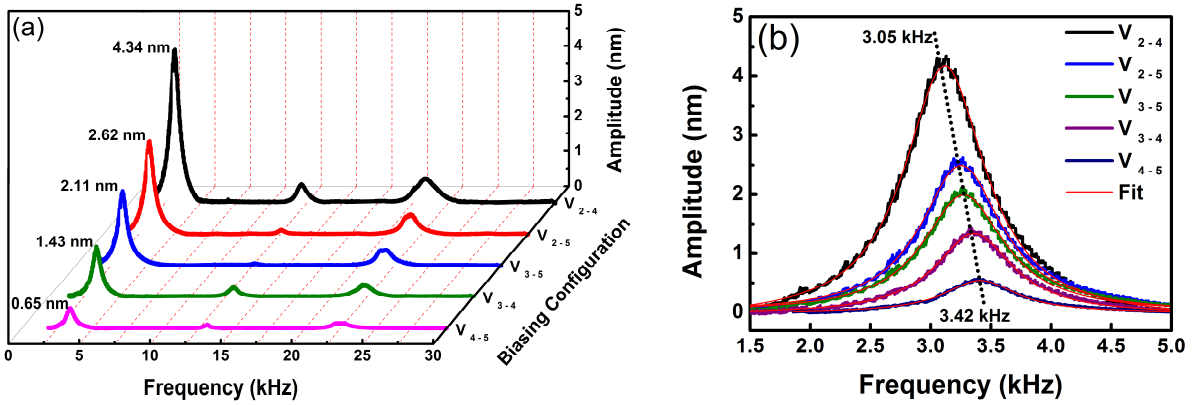

FIG. 3. The frequency response of 350 nm-thick circular membranes to different biasing configurations (a) full spectra and (b) first resonant frequency.

In summary, ultra-large graphene-based bilayer thin films with ultra-large diameter to thickness aspect ratio of ~ 10,000 have been realized experimentally and actuated electrothermally. Thin films consisting of multilayer graphene and 350 – 500 nm-thick PMMA have been transferred to circular cavities with a diameter of 3.5 mm. The dynamic response of the bilayer thin films has been investigated electrothermally by driving the structures with a combination of AC and DC actuation voltages. The analytical models have shown that the bilayer structure with the given aspect ratio in this work acts like a membrane rather than a plate. A resonant frequency of 3.26 kHz has been achieved for 350 nm-thick membranes. The actuation results reveal that the resonant frequency and the amplitude of vibration can be influenced significantly by the driving configurations. A downward shift of –108187 ppm in the first resonant frequency and the highest vibration amplitude of 4.34 nm have been induced in the 350 nm-thick membranes when the input driving current passes through the center of the membrane. The results indicate that low frequency within the audio regime (20 Hz – 20 kHz) is achievable with the design of large and thin membranes, promising practical audio applications for headphones, speakers, microphones and hearing aid devices.

See supplementary material for further information about electrothermal actuation, 3D images of the first three resonant modes for circular membranes measured by LDV, and analytical model of circular plate.

The authors acknowledge the financial support of UK Engineering and Physical Sciences Research Council (EPSRC). The Ministry of Higher Education and Scientific Research (MOHESR) of Iraq is acknowledged for the financial support through the PhD scholarship program of the first author.

[1] C. Chen, S. Lee, V. V. Deshpande, G.-H. Lee, M. Lekas, K. Shepard, and J. Hone, Nat. Nanotechnol. **8**, 923 (2013).

[2] S.E. Zhu, R. Shabani, J. Rho, Y. Kim, B.H. Hong, J.H. Ahn, and H.J. Cho, Nano Lett. **11**, 977 (2011).

[3] J. Aguilera-Servin, T. Miao, and M. Bockrath, Appl. Phys. Lett. **106**, 83103 (2015).

[4] M. Pumera, Mater. Today **14**, 308 (2011).

[5] D. Todorović, A. Matković, M. Milićević, D. Jovanović, R. Gajić, I. Salom, and M. Spasenović, 2D Mater. **2**, 45013 (2015).

[6] Q. Zhou and A. Zettl, Appl. Phys. Lett. **102**, 223109 (2013).

[7] Q. Wang, W. Hong, L. Dong, H.W. Lin, L.T. Liu, T.L. Ren, A.R.H. Walker, G.J. Cheng, C.A. Hacker, C.A. Richter,

Q.L. Li, D.J. Gundlach, and X.L. Liang, Nanoscale **8**, 7663 (2016).

[8] A. Balan, C.-C. Chien, R. Engelke, M. Drndić, and A. Ouerghi, Sci. Rep. **5**, 17775 (2016).

[9] S. Woo, J.H. Han, J.H. Lee, S. Cho, K.W. Seong, M. Choi, and J.H. Cho, ACS Appl. Mater. Interfaces **9**, 1237 (2017).

[10] M. Younis, *Sensing and Actuation Actuation in MEMS* (Springer US, 2011).

[11] G. Müller and M. Möser, *Handbook of Engineering Acoustics* (Springer Berlin Heidelberg, 2013).

[12] C.N. Lau, W. Bao, and J. Velasco, Mater. Today **15**, 238 (2012).

[13] A.A. Balandin, S. Ghosh, W. Bao, I. Calizo, D. Teweldebrhan, F. Miao, and C.N. Lau, Nano Lett. **8**, 902 (2008).

[14] L. Xu and I.K. Oh, Composites **7978**, 79781V (2011).

[15] H. Liu, D. Niu, W. Jiang, T. Zhao, B. Lei, L. Yin, Y. Shi, B. Chen, and B. Lu, Sensors Actuators A Phys. **239**, 45 (2016).

[16] R.A. Barton, B. Ilic, A.M. van der Zande, W.S. Whitney, P.L. McEuen, J.M. Parpia, and H.G. Craighead, Nano Lett. **11**, 1232 (2011).

[17] A. Castellanos-Gomez, V. Singh, H.S.J. van der Zant, and G.A. Steele, Ann. Phys. **527**, 27 (2015).

[18] P. Kanjanaboos, X.M. Lin, J.E. Sader, S.M. Rupich, H.M. Jaeger, and J.R. Guest, Nano Lett. **13**, 2158 (2013).

[19] H. Schlicke, C.J. Schröter, and T. Vossmeyer, Nanoscale **8**, 15880 (2016).

[20] Y. Zhou and F. Amirouche, Int. J. Adv. Manuf. Technol. **45**, 1187 (2009).

Supplementary Material:

Dynamic behavior of ultra large graphene-based membranes using electrothermal transduction

A. Al-mashaal[1)] G. S. Wood[1)] A. Torin[2)] E. Mastropaolo[1)] M. J. Newton[2)] and R. Cheung[1)]

[1]*School of Engineering, Institute for Integrated Micro and Nano Systems, University of Edinburgh, Edinburgh EH9 3FF, UK*

[2]*Acoustics and Audio Group, University of Edinburgh, Edinburgh EH9 3JZ, UK*

1. Electrothermal actuation

The graphene/PMMA bilayer thin films can be driven into resonance by applying a combination of alternating current (AC) and direct current (DC) voltages (V_{ac} and V_{dc}) to the actuation electrodes. The relationship between the applied voltage V and dissipated power P in a resistance R is given as ($P = V^2/R$). Therefore, when the actuation voltages applied, the corresponding V^2 is given by[1]:

$$V^2 = 2V_{ac}V_{dc}\sin\omega_{ac}t + 0.5V_{ac}^2\,(1 - \cos 2\omega_{ac}t) + V_{dc}^2 \tag{S1}$$

where ω_{ac} is the angular frequency of the input voltage V_{ac}. When the actuation voltage is a combination of both V_{ac} and V_{dc}, the membrane is driven into resonance when the driving frequency of the input voltage f_{ac} matches the mechanical resonant frequency of the membrane f_0 (i.e. $f_{ac} = f_0$). When the applied voltage is only V_{ac}, the resonance takes place at $f_{ac} = 1/2f_0$.

2. Thermal response of the actuator

The change in the average temperature ΔT can be influenced by the thermal conductivity and dissipated power[2]. Since graphene has higher thermal conductivity than PMMA and due to the inverse proportionality of the thermal response time τ to the average thermal diffusivity d_{avg} (i.e. $\tau = 1/d_{avg}$)[3], it is highly possible to achieve fast thermal response to the conductive heat.

3. Shapes of the measured modes:

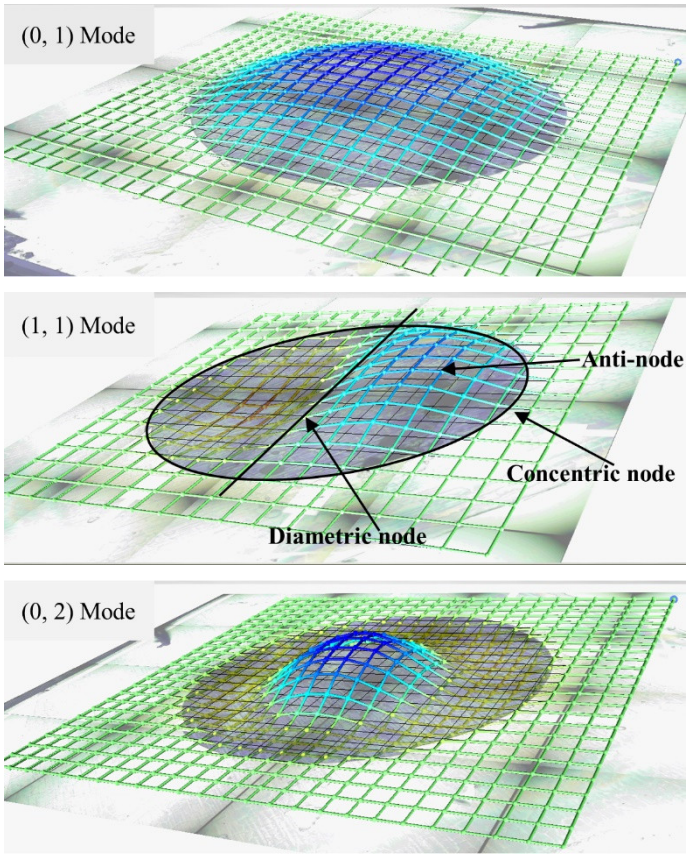

Fig. S1. The first three shape of the resonant modes for circular membranes measured by LDV.

4. Resonant frequency of circular plate structures

The resonant frequency of clamped, stress-free circular plate can be written as[6]:

$$f_{mn}(plate) = \frac{\beta_{mn}}{2\pi R^2}\sqrt{\frac{D}{\rho t}} \tag{S2}$$

where R is the radius of the membrane, D is bending rigidity$\left(D = \frac{Et^3}{12(1-\nu^2)}\right)$, E is Young's modulus, ν is Poisson's ratio, t is the total thickness of the membrane, ρ is the density of the material, and β_{mn} is a dimensionless dimensionless coefficient of the resonant mode. For bilayer plate, the effective values of parameters of Young's modulus E_{eff}, thickness t_{eff}, density ρ_{eff}, and bending rigidity D_{eff} of the composite membranes of graphene (g) and PMMA (p) can be expressed as follows[7,8]:

$$E_{eff} = \frac{E_g t_g + E_p t_p}{t_g + t_p} \tag{S3}$$

$$t_{eff} = t_g + t_p \tag{S4}$$

$$\rho_{eff} = \frac{\rho_g t_g + \rho_p t_p}{t_g + t_p} \tag{S5}$$

$$D_{eff} = \frac{\hat{E}_g\left(\left(t_g - K\right)^3 + K^3\right)}{3} + \frac{\hat{E}_p\left(\left(t_p + t_g - K\right)^3 - \left(t_g - K\right)^3\right)}{3} \tag{S6}$$

where $\hat{E}_g = \frac{E_g}{(1-\nu_g^2)}, \hat{E}_p = \frac{E_p}{(1-\nu_p^2)}$, $K = \frac{\hat{E}_g t_g^2 + \hat{E}_p\left(\left(t_g+t_p\right)^2 - {t_g}^3\right)}{2(\hat{E}_g t_g + \hat{E}_p t_p)}$.

By including the thermal stress (σ_t) and the surrounding medium mass (A_m), the resonant frequency of clamped bilayer circular plate can be written as follows:

$$f_{mn}(plate) = \frac{\beta_{mn}}{2\pi R^2}\sqrt{\frac{D_{eff} + \sigma_t}{\rho_{eff} t_{eff}(1 + A_m)}} \tag{S7}$$

where ρ_{eff} is the effective density of the bilayer materials, and D_{eff} is the effective bending rigidity of the film.

5. Thermal stress from the plate model

If the transferred films are assumed to behave as plates, the calculated resonant frequencies from the stress-free plate model are not in agreement with the measurements (see table SI). If thermal stress is included in the plate model (equation S7), the experimental resonant frequency fits with the model at only extremely high values of stress (e.g. 135.53 GPa for 350 nm-thick film). Such a high stress seems unlikely to be induced practically at an electrothermal actuation voltage of 8 V. Therefore, our bilayer structure is more likely to behave as a membrane rather than a plate.

Table SI. Estimation of the magnitude of (stress) and strain in the graphene/PMMA films with different thicknesses based on the experimental measurements and plate model in equation (S7) for the first resonant frequency ($f_{0,1}$). The strain has been calculated based on the estimated values of stress.

Graphene/ PMMA Thickness	**Analytical**			**Experimental**
	Stress (GPa)	**Strain**	$\boldsymbol{f_{0,1}}$ (kHz)	$\boldsymbol{f_{0,1}}$ (kHz)
8 layers/ 350 nm	0	-	0.09	3.26
8 layers/ 400 nm	0	-	0.07	3.73
8 layers/ 500 nm	0	-	0.06	4.64
8 layers/ 350 nm	135.53	11.68	3.26	3.26
8 layers/ 400 nm	182.57	17.18	3.73	3.73
8 layers/ 500 nm	298.43	32.19	4.64	4.64

[1] L. Jiang, R. Cheung, J. Hedley, M. Hassan, A.J. Harris, J.S. Burdess, M. Mehregany, and C.A. Zorman, Sensors Actuators A Phys. **128**, 376 (2006).

[2] E. Mastropaolo, G.S. Wood, I. Gual, P. Parmiter, and R. Cheung, J. Microelectromechanical Syst. **21**, 811 (2012).

[3] S. Pal and H. Xie, J. Micromechanics Microengineering **22**, 115036 (2012).

[4] S.P. Timoshenko, *Vibration Problems in Engineering.*, Third edit (New York, 1955).

[5] M.A. Maden, A. Jagota, S. Mazur, and R.J. Farris, J. Am. Ceram. Soc. **77**, 625 (1994).

[6] O. Brand, S.M. Dufour, Isabelle Heinrich, and F. Josse, *Resonant MEMS : Fundamentals, Implementation and Application* (Wiley-VCH Verlag & Co. KGaA, 2015).

[7] A. Cabal, D.S. Ross, J.A. Lebens, and D.P. Trauernicht, Sensors Actuators A Phys. **123–124**, 531 (2005).

[8] X. Zhuang, A. Nikoozadeh, M.A. Beasley, G.G. Yaralioglu, B.T. Khuri-Yakub, and B.L. Pruitt, J. Micromechanics Microengineering **17**, 994 (2007).